Turkish Journal of Electrical Engineering & Computer Sciences

http://journals.tubitak.gov.tr/elektrik/

Research Article

Turk J Elec Eng & Comp Sci
(2016) 24: 4208 – 4217

doi:10.3906/elk-1501-154

High photoresponse from solution processed conventional and inverted ultraviolet photodetectors

Görkem MEMİŞOĞLU[1,2,*], **Canan VARLIKLI**[1,*]
[1]Solar Energy Institute, Ege University, Bornova, İzmir, Turkey
[2]Vestel Electronics, MOS, Manisa, Turkey

Received: 21.01.2015 • **Accepted/Published Online:** 28.07.2015 • **Final Version:** 20.06.2016

Abstract: The optical and electrical properties of conventional and inverted type ultraviolet photodetectors (UVPDs) with active layers of poly(9,9-dioctylfluorenyl-2,7-ylenethynylene (PFE), N,N'-bis-n-butyl-1,4,5,8-naphthalenediimide (BNDI), and zincoxide (ZnO) are introduced. Optimized devices showed high photoresponse, external quantum efficiency (EQE), and detectivity (D*) values. Under 365 nm 1 mW/cm^2, the conventional device (ITO/PEDOT:PSS/[(PFE:BNDI) (3:1):8 wt% ZnO]/Al) and the inverted device (ITO/[(PFE:BNDI)(3:1):8 wt% ZnO]/Au) gave photoresponsivities of 515 mA/W and 316 mA/W, D* of 1.12 $\times$ 10^{14} *Jones* and 0.71 $\times$ 10^{14} *Jones*, and EQE of 174% and 107%, respectively. Annealing the devices at polymer's glass transition temperature (T$_g$ 60 $^\circ$ C), enhanced these values to 651 mA/W and 343 mA/W, 1.33 $\times$ 10^{14} *Jones* and 0.73 $\times$ 10^{14} *Jones*, and 221% and 116%, respectively. Furthermore, high performance, sensitivity, D*, and EQE values of different architectures were examined by impedance spectroscopy.

Key words: Ultraviolet photodetector, hybrid system, zinc oxide nanoparticle, polymer, impedance spectroscopy

1. Introduction

UV radiation photodetectors (PDs) are promising devices in the optoelectronics world with their importance in application areas such as health, automotive and chip industries, military, space communication, and academic research [1–4]. Obtaining higher efficiency and longer stability of UV PDs depends upon the optical and electrical performances of the semiconductor materials used and the UV PD architecture. Commercially available devices are based on inorganic semiconductors [e.g., silicon carbide, gallium phosphide, gallium nitride (GaN)]. However, their manufacturing is not cost effective and their responsivity values are low. To the best of our knowledge, maximum photoresponse is 180 mA/W under 360 nm wavelength of radiation for an active area of 0.5 mm^2 of a GaN based UV PD [5]. Solution processable organic semiconductors may not only provide a solution to the cost problem of current technology, but also have the potential of increasing the responsivity values with their high molar absorptivity constants at the UV range. However, responsivity and stability are still the main parameters that should be compared/competed with the corresponding inorganic semiconductor based technology.

Polyfluorene (PF) type polymer is a p-type organic semiconducting material with hole mobility (10^{-3}–10^{-4} cm^2/Vs) [6], and naphthalenediimide (NDI) is an n-type, strong UV absorber organic semiconductor material with electron mobility of 10^{-2} cm^2/Vs [7]. These two materials presented a good correlation; presence of NDI in the polymer increased the absorbance at 365 nm and caused a quenching of the excited state electrons.

*Correspondence: canan.varlikli@ege.edu.tr, gorkemgrkm@yahoo.com

Optimization of the polymer:NDI weight ratio resulted in a high photoresponse of 410 mA/W under 1 mW/cm^2 365 nm light at –4 V [8]. Further attempts to increase the photoresponse have been carried out by the addition of nitrogen doped TiO_2 and the results were promising: 597 mA/W under 1 mW/cm^2 365 nm UV light at –4 V [9].

ZnO is an n-type material with 10^{-2} cm^2/Vs electron mobility [10]. It is introduced as a potential alternative for photonic applications and possesses transparency to visible (transmission between 400 and 800 nm is nearly 92%) [11]. ZnO is one of the most studied n-type metal oxide semiconductor materials with its large direct bandgap (nearly 3.3 eV). The literature contains many reports on its comparison with TiO_2 for many different application areas: antibacterial activity [12], photocatalytic degradation [13,14], solar cell performance [15,16], etc. Although in many of them ZnO presented comparable activity with TiO_2, regarding the photocurrent performances the literature contains controversial reports [15,16]. Within those reports the study by Dindar and Icli is one of the most important ones that presents the advantages of ZnO over TiO_2 [14].

The present study aims to enhance the UV-PD performance of a solution processed PF:NDI based active layer through enhanced charge generation and collection and monitor the stability of the device that presented better performance. With this motivation, conventional and inverted UV PDs with the active layer of PF:NDI:ZnO are prepared. In both of the architectures, exciton generation starts with the absorption of light by the active layer. Then diffusion and charge separation occur. Electron collection is provided through a cathode [such as aluminum (Al)] and an anode [such as indium tin oxide (ITO)] in the conventional and inverted system, respectively.

Photoresponse and detectivity (D*) values, which are dependent on the photocurrent, and both photo and dark currents, respectively, are calculated. Deep electrical analysis of the responsivity and stability differences of different device architectures is investigated. Obtained responsivity values are more than threefold those of the commercially available UV PDs but stability is still an issue.

2. Experimental

Indium tin oxide (ITO) coated glass substrates (Delta Technologies, 4–10 $\Omega/\Box$) were etched and cleaned by the general chemical method [8,9]. O_2 plasma was applied for 5 min before coating of the next layer. For the conventional device structure, poly(3,4-ethylenedioxythiophene):poly(styrenesulfonate) (PEDOT:PSS) was spin-coated at 3000 rpm for 1 min and vacuum dried at 100 ° C for 30 min, resulting in a film thickness of 45 nm. For the active layer of the conventional structure, poly(9,9-dioctylfluorenyl-2,7-yleneethynylene (PFE), N,N'-bis-n-butyl-1,4,5,8-naphthalenediimide (BNDI), and ZnO NPs (synthesized as reported by Chieng et al. [17]) are used and PFE:BNDI:ZnO solutions were spin coated at 1500 rpm onto the PEDOT:PSS layer. Finally, the Al electrode (80 nm) was deposited by using a shadow-mask with vacuum thermal evaporator attached to an MBRAUN 200B glove box system with a depositing rate of 0.5 Å/s at 3×10^{-6} mbar pressure. For the inverted device structure, PFE:BNDI:ZnO solutions were directly spin coated onto ITO substrates and the Au electrode (50 nm) was deposited with the same shadow-mask at the same rate and pressure as that of the Al in conventional system. All of the chemicals used were provided by Sigma Aldrich.

The stock solution of [(PFE:BNDI) (3:1)] was prepared in chloroform and doping ratios of 7, 8, 9, and 10 wt% of ZnO nanoparticles (NPs) were used for the active layers. Thicknesses were independent of the NP content, and were around 85 nm. The UV-PD device structures studied were ITO/PEDOT:PSS/[(PFE:BNDI)(3:1): x wt% ZnO]/Al (x: 7, 8, 9, and 10) and ITO/[(PFE:BNDI)(3:1): x wt% ZnO]/Au (x: 7, 8, 9, and 10) with

the active area of 12 mm^2. Five parallel measurements were performed for each device. The active layer of the device that presented the highest responsivity was annealed, before the final layer evaporation, for 15 min at the T_g of polymer ($T_g^{PFE} = 60\ ^\circ$ C [9]). Electrical characterizations were performed in a glove box under nitrogen environment. Ground and excited state energy levels of PFE, BNDI, and ZnO are taken from the literature [9,18].

PerkinElmer UV-Vis-NIR and Edinburgh FLS920P spectrophotometers were used for performing the absorption and photoluminescence (PL), respectively. The preparation of organic coatings was performed by a Laurell WS-400B-6NPP-LITE spin coater and the thicknesses of thin films were determined by an Ambios XP-1 high resolution surface profilometer. Film morphology monitoring was performed by an Ambios QScope 250 model atomic force microscope (AFM). A Keithley 2400 source meter and an IM6 Zahner Elektrik impedance analyzer were used for current-voltage (I-V) and impedance characteristics of the PDs, respectively. Illumination was provided by a solar simulator attached to the glove box system and the intensity is measured by a Nova II versatile laser power energy display that contains a calibrated silicon photodiode. Solar simulator irradiation is filtered through 365 nm bandpass interference filter with $\pm$ 10 nm of full width at half maximum that was obtained from Edmund Optics.

3. Results and discussion

The optical characterization starts with the measurement of absorbance and PL intensities. Absorption and PL spectra of 1500 rpm spin-casted [(PFE:BNDI)(3:1): x wt % ZnO], x: 7, 8, 9, and 10 thin films on quartz substrates are given in Figures 1a and 1b, respectively. The absorbance of PFE:BNDI (3:1) blend is enhanced by the addition of ZnO NPs with no spectral shifts and reached its maximum with 8 wt% ZnO NP doping, as shown in Figure 1a. In most of the manuscripts published on PD application of ZnO blends this result is attributed to scattering effects [19,20]. However, if this had been the only effect, we should not have observed any reduction with the continuing increment in ZnO content [18]. Yet, for the 9 and 10 wt% doping ratios of ZnO a decrease in the absorbance is monitored. We have attributed this result to the trapping effect of ZnO and it was supported by the impedance measurements [18]. Therefore, we may say that the presence of BNDI did not cause a difference in the ground state behavior of the PFE:ZnO blend. However, as presented in Figure 1b, the presence of BNDI in the PFE:ZnO blend caused a significant quenching, which indicates that the energy

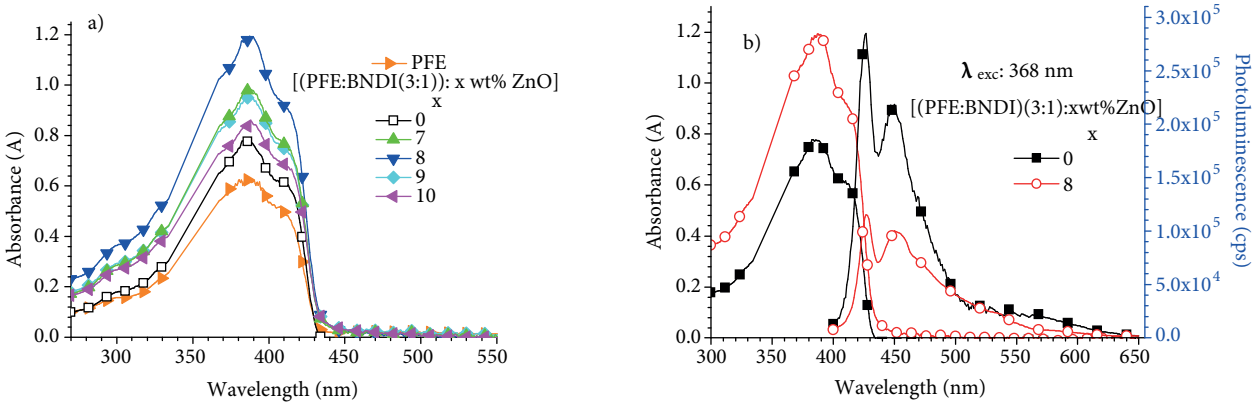

Figure 1. a) Absorption spectra of PFE and (PFE:BNDI)(3:1):x wt% ZnO, (x: 0, 7, 8, 9, and 10) blends; b) absorption and photoluminescence spectra of (PFE:BNDI) and (PFE:BNDI)(3:1):8 wt% ZnO blends on quartz substrates (λ_{exc} = 368 nm).

transfer mechanism proposed in our manuscript on PFE:BNDI:TiO_2 [9] is also valid for the PFE:BNDI:ZnO blend.

Electrical characterizations are performed on conventional and inverted UV PDs. Device structures and energy levels are shown in Figures 2a and 2b, respectively. For conventional and inverted PDs, the measured dark and light current density (J, mA/cm^2) versus voltage (V) curves characteristics at 1 mW/cm^2 at 365 nm for the voltage range of –4 V to 4 V are shown in Figures 3a and 3b, respectively, and the electrical performance values are summarized in Tables 1 and 2. Currents under UV light illumination were 10^4 times larger than dark current at –4 V bias, for both conventional and inverted UV PDs. The low dark current implies better noise performances. According to the photocurrent investigation of devices, 8 wt% ZnO doped unannealed conventional and inverted PDs showed maximum J values of 0.515 mA/cm^2 and 0.316 mA/cm^2, respectively at –4 V applied potential. These values correspond to photoresponsivity values of 515 mA/W and 316 mA/W and increase to 651 mA/W and 343 mA/W with annealing of active layers of the conventional and inverted device structures, respectively. As expected, the photoresponsivity value obtained by the conventional device structure is higher than that of the inverted one. A dramatic decrease in current density is observed, over 8 wt% ZnO doping (9 wt% and 10 wt%) in both conventional and inverted PDs, which can be attributed to the lower absorption intensities (Figure 1a). The photoresponsivity values of the conventional device are comparable with those of the commercial UV-PDs and much higher than the value we could obtain with solution processed UV-PD with the active layer of PFE:BNDI:TiO_2; i.e. 156 mA/W for the pure TiO_2, 545 mA/W for the nitrogen doped TiO_2, which was further increased to 597 mA/W with annealing [9]. From this point of the manuscript PFE:BNDI:TiO_2 refers the device prepared with pure TiO_2 doping.

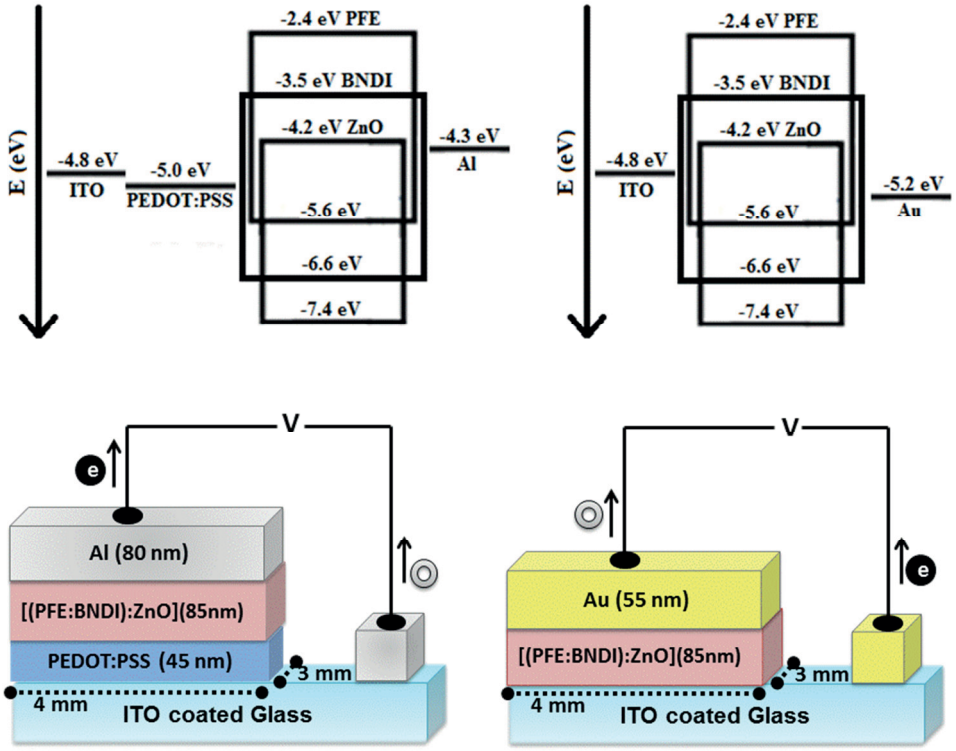

Figure 2. Device structures and energy levels of a) conventional and b) inverted type UV PDs.

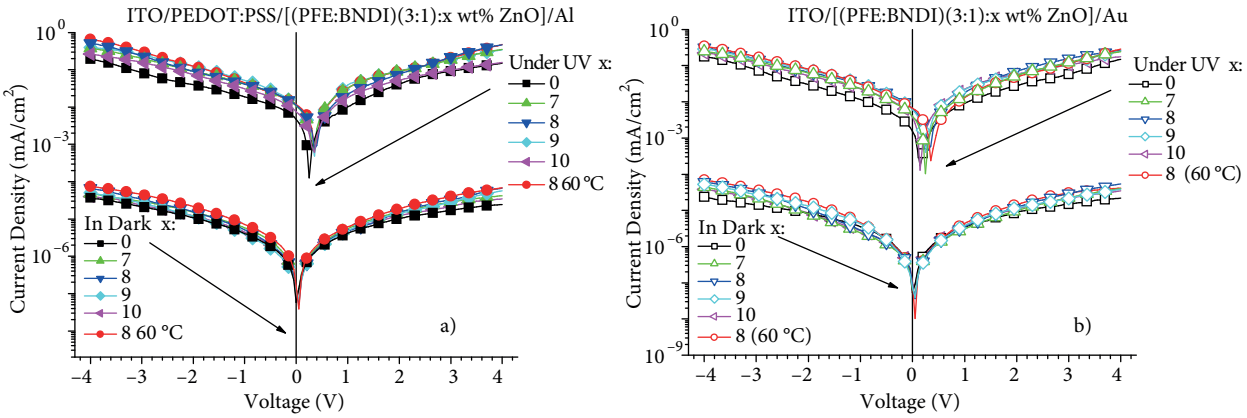

Figure 3. Current density versus voltage curves, of a) conventional and b) inverted devices, obtained in the dark and under 1 mW/cm^2 at 365 nm wavelength.

Table 1. Electrical parameters of conventional devices.

Parameters	ITO/PEDOT:PSS/[(PFE:BNDI)(3:1):x wt% ZnO]/Al					
	RT					60 ° C
	0	7	8	9	10	8
R (mA/W)	192	379	515	392	262	651
R_p (kΩ)	48.3	38.0	26.2	31.1	40.3	20.3
R_s (kΩ)	0.139	0.138	0.137	0.139	0.139	0.130
mu (cm^2/V.s)(× 10^8)	0.62	1.4	2.9	2.29	1.1	3.6
J_{light}(at –4 V)(mA/cm^2)	0.192	0.379	0.515	0.392	0.262	0.651
J_{dark}(at –4 V)(mA/cm^2)(× 10^5)	3.64	4.79	6.62	5.00	4.02	7.51
J_{dark}(at 0 V)(mA/cm^2)(× 10^8)	5.76	9.16	13.5	11.5	7.41	15.8
EQE (at –4 V) (%)	65	128	174	133	88	221
D* (at –4 V)(Jones)(× 10^{-14})	0.56	0.96	1.12	0.98	0.73	1.33

Table 2. Electrical parameters of inverted devices.

Parameters	ITO / [(PFE:BNDI)(3:1):x wt% ZnO] / Au					
	RT					60 ° C
	0	7	8	9	10	8
R (mA/W)	177	248	316	285	227	343
R_p (kΩ)	66.6	44.9	29.8	36.6	53.0	23.7
R_s (kΩ)	0.145	0.141	0.140	0.143	0.144	0.134
mu (cm^2/V.s) (× 10^8)	0.55	0.99	1.38	1.23	0.73	2.16
J_{light}(at –4 V) (mA/cm^2)	0.212	0.248	0.315	0.286	0.226	0.343
J_{dark}(at –4 V)(mA/cm^2)(× 10^5)	2.35	4.41	6.14	4.95	2.92	6.93
J_{dark}(at 0 V)(mA/cm^2)(× 10^8)	5.32	6.83	9.51	7.59	6.54	10.4
EQE (at –4 V) (%)	60	84	107	97	76	116
D* (at –4 V)(Jones) (× 10^{-14})	0.64	0.68	0.71	0.69	0.65	0.73

UV PD sensitivity (S) value, which is equal to the contrast ratio of devices, is calculated with

$$S = \frac{\mathbf{I_{ill}}}{\mathbf{I_{dark}}}, \tag{1}$$

where I_{ill} is the photocurrent and I_{dark} is the dark current [21]. Calculated sensitivities for 8 wt% doped devices of conventional and inverted PDs at –4 V are 7.7 $\times$ 10^3 and 0.1 $\times$ 10^3 at room temperature, and these values increase to 8.6 $\times$ 10^3 and 0.9 $\times$ 10^3 with annealing. Sensitivity values are comparable with the literature [21,22]. In order to understand the background of these performances, impedance spectroscopy is applied [23,24]. Figures 4a and 4b show the impedance curves of the conventional and inverted PDs, which contained different amounts of ZnO in PFE:BNDI blend, under UV light. Between 1 Hz and 1 MHz frequency regions, Nyquist plots showed single semicircles for all devices, which can be described by a parallel resistance (R_p) and capacitance (C_p), with a serial resistance (R_s). R_s, which generates from the interface of ITO and the organic layer, showed nearly the same values for both conventional and inverted device structures (0.130–0.145 kΩ) (Tables 1 and 2). Parallel resistance (R_p) generates from the bulk of the device. For both of the device structures minimum R_p values are obtained with 8 wt% ZnO doping and they were further reduced by annealing (Tables 1 and 2; Figure 4). Although the lowest R_p values belong to the 8 wt% ZnO doped annealed devices in conventional and inverted UV PDs, the conventional device, which has the highest absorption intensity, has the lowest R_p (20.3 Ω). For higher doping ratios, 9 wt% and 10 wt%, ZnO starts acting as a trap for the photogenerated charges and causes an increase in the R_p values and a consequent decrease in photoresponsivity. By using the impedance spectroscopy, transit time (τ_t) of charge carriers of the PD is calculated with the susceptance (–ΔB) method [25] and total charge carrier mobility (mu) is calculated with

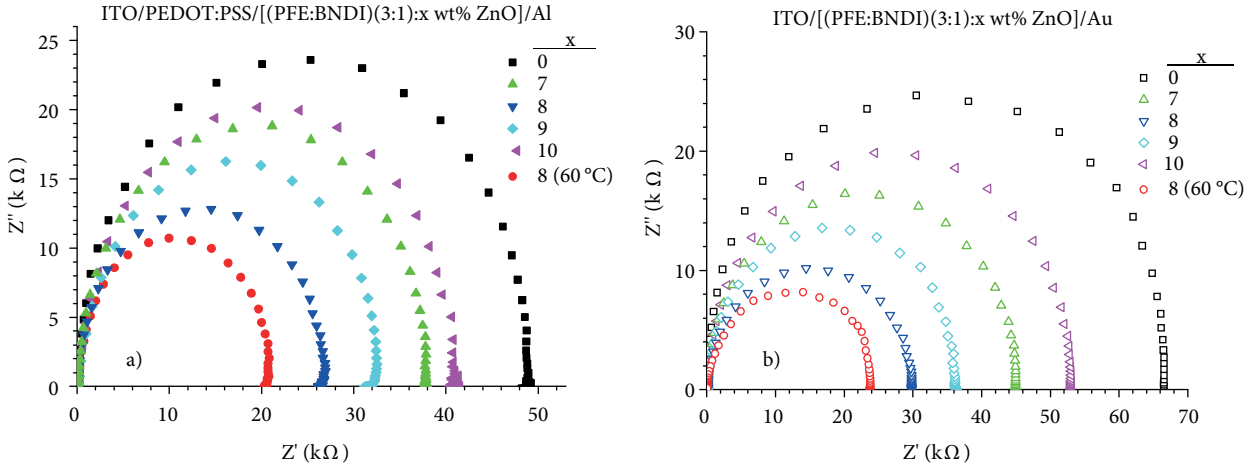

Figure 4. Impedance curves of a) conventional and b) inverted devices, obtained under 1 mW/cm^2 at 365 nm wavelength under –4 V bias.

$$\mu = \frac{4L^2}{3\tau_t V}, \tag{2}$$

where L is the thickness of the active layer and V is potential. Calculated mobility values are shown in Tables 1 and 2. For 8 wt% ZnO doping, the conventional UV PD presented a total charge mobility value more than 2 times higher than that of the inverted UV PD. In their study comparing the electron transfer properties of ZnO and TiO_2, Cell et al. have found that the optimization of metaloxide thickness results in approximately the same short circuit currents and concluded that electron transport rate is faster in ZnO [15]. If we evaluate the

photodetector performances presented in this study together with formerly published PFE:BNDI:TiO_2 device, we may also attribute the better performance of both conventional and inverted device architectures with the active layer of PFE:BNDI:ZnO to better charge transport mobility; i.e. $mu = 0.51 \times 10^{-8}$ cm^2/V.s for PFE:BNDI:TiO_2 [9].

External quantum efficiency (EQE), which is the ratio of the collected charge carriers to the number of photons, is calculated according to literature with

$$EQE = \frac{hcI}{e\lambda P}, \tag{3}$$

where h is the Planck's constant, c is the speed of light in a vacuum, I is the photocurrent, e is the electron charge, λ is the light wavelength, and P is the power of the light [26]. ZnO concentration dependent EQEs of conventional and inverted PDs are shown in Figure 5a. EQE values are 65% and 60% for the bare conventional and inverted PDs, respectively. These values are increased to 174% and 107% at RT and reached 221% and 116% with annealing (at 60 ° C) for conventional and inverted 8 wt% ZnO doped PDs, respectively. D* values versus ZnO concentration of conventional and inverted PDs under 1 mW/cm^2 illumination at 365 nm wavelength at –4 V are shown in Figure 5b. D* is determined by

$$D* = \frac{R}{\sqrt{2qJ_{dark}}}, \tag{4}$$

where R is the photoresponsivity, q is the charge of the electron, and J_{dark} is the dark current density [26]. The 8 wt% ZnO doped PDs presented D* values of 1.12×10^{14} *Jones* and 0.71×10^{14} *Jones* at RT, and 1.33×10^{14} *Jones* and 0.73×10^{14} *Jones* at 60 ° C for conventional and inverted PD structures. EQE and also D* values are comparable with literature values [19].

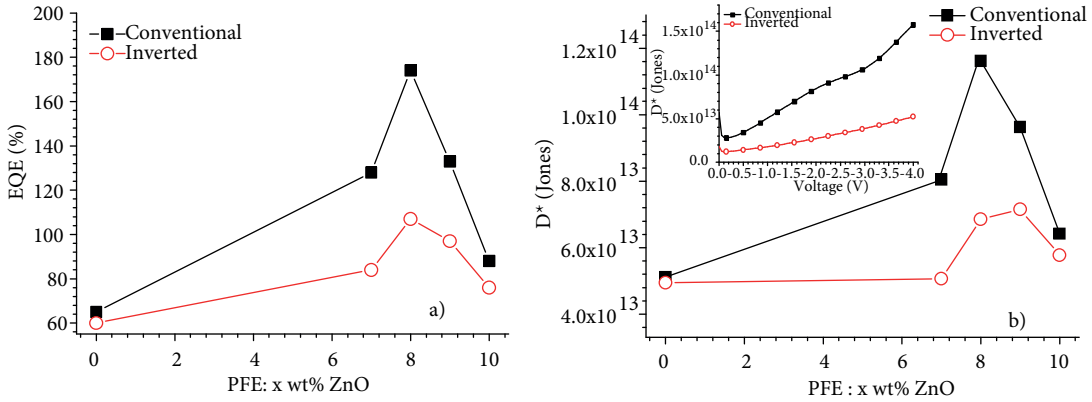

Figure 5. Concentration dependent a) EQE, and b) Detectivity (inset: detectivity values for the best performance (8 wt% ZnO doped) devices) values of conventional and inverted photodetectors for [(PFE:BNDI)(3:1)): x wt% ZnO] active layer under 1 mW/cm^2 at 365 nm wavelength.

Photoresponsivities under 0.2, 0.5, 1, 1.5, 2, and 2.5 mW/cm^2 365 nm UV light intensities are also investigated and presented saturation over 1.5 mW/cm^2 for both of the devices (Figure 6a). Time dependent photoresponsivity characters under 1 mW/cm^2 365 nm of the conventional and inverted PDs for [(PFE:BNDI)(3:1)):8

wt% ZnO] active layer are shown in Figure 6b. After 180 min, inverted PD responsivity is nearly stabilized. Lower photoresponse and higher stability of inverted device structures are reported in the literature and our results are in accordance with them [18–20,23,27–29].

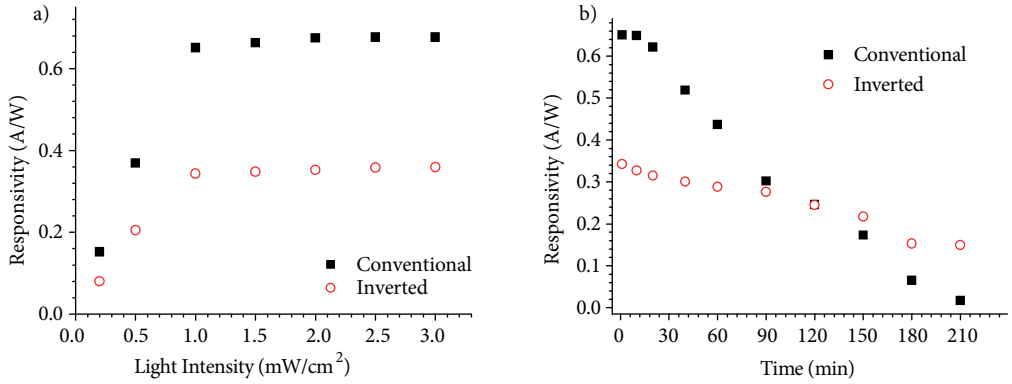

Figure 6. Photoresponsivity values of conventional and inverted photodetectors a) under different excitation intensities, and b) time dependent values under 1 mW/cm^2 at 365 nm wavelength.

4. Conclusion

Under illumination intensity of 1 mW/cm^2 at 365 nm and applied potential of –4 V, conventional (ITO/PEDOT:PSS/[(PFE:BNDI)(3:1):8 wt% ZnO]/Al) and inverted (ITO/[(PFE:BNDI)(3:1):8 wt% ZnO]/Au) UV-PD devices gave photoresponsivities of 515 mA/W and 316 mA/W, respectively. Annealing the devices at polymer's glass transition temperature (T_g 60 ° C) enhanced these values to 651 mA/W and 343 mA/W, respectively. When compared to the formerly reported UV-PD performance of the device with PFE:BNDI:TiO_2 [9], both conventional and inverted device architectures of PFE:BNDI:ZnO active layer presented better photoresponse values. In the above discussions, this finding is attributed to the better charge mobility in ZnO. However, in order to understand whether there are any other morphological, spectroscopic, or electrical reasons for those effects on this result, additional measurements, e.g., FESEM and transient absorption, need to be performed, but are not within the scope of this manuscript. Although the photoresponsivity values are quite promising, stability of solution processed monolayer organic UV-PDs needs much enhancement in order for them to become comparable with the commercially available competitors.

Acknowledgment

The authors are thankful to Prof Dr Sıddık İçli, who retired from Ege University Solar Energy Institute (EU-SEI) in 2014 and made valuable contributions to the organic electronic research infrastructure.

References

[1] Yu G, Pakbaz K, Heeger AJ. Semiconducting polymer diodes: large size, low cost photodetectors with excellent visible-ultraviolet sensitivity. Appl Phys Lett 1994; 64: 3422-3424.

[2] Gong X, Tong M, Xia Y, Cai W, Moon JS, Cao Y Yu G, Shieh CL, Nilsson B, Heeger AJ. High-detectivity polymer photodetectors with spectral response from 300 nm to 1450 nm. Science 2009; 325: 1665-1667.

[3] Lee ML, Mue TS, Huang FW, Yang JH, Sheu JK. High-performance GaN metal-insulator-semiconductor ultraviolet photodetectors using gallium oxide as gate layer. Opt Express 2011; 19: 12658-12663.

[4] Baeg KJ, Binda M, Natali D, Caironi M, Noh YY. Organic light detectors: photodiodes and phototransistors. Adv Mat 2013; 25: 4267-4295.

[5] Sungmook. Lim, Long Term Stability Testing of GaN (gallium nitride) based UV sensor under UV lamp irradiation, 2011.

[6] Tinti F, Debebe SE, Mammo W, Yohannes T, Camaioni N. Temperature and electric field dependent hole mobility in a polyfluorene copolymer. Synth Met 2011; 161: 794-798.

[7] Singh TB, Erten S, Günes S, Zafer C, Turkmen G, Kuban B, Teoman Y, Sariciftci NS, Icli S. Soluble derivatives of perylene and naphthalene diimide for n-channel organic field-effect transistors. Org Electron 2006; 7: 480-489.

[8] Memisoglu G, Varlikli C. Highly efficient organic UV photodetectors based on polyfluorene and naphthalenediimide blends: effect of thermal annealing. Int J Photoenergy 2012; 2012: 1-11.

[9] Memisoglu G, Varlikli C, Diker H. Solution-processed polyfluorene: naphthalenediimide-N-doped TiO_2 hybrids for ultraviolet photodetector applications. J Electron Mater 2013; 42: 3502-3511.

[10] Jin Z, Wang J. High-responsivity solution-processed organic-inorganic hybrid bilayer thin film photoconductors. J Mater Chem C 2013; 1: 7996-8002.

[11] He JH, Lin YH, McConney ME, Tsukruk VV, Wang ZL, Bao G. Enhancing UV photoconductivity of ZnO nanobelt by polyacrylonitrile functionalization. J Appl Phys 2007; 102: 084303-4.

[12] Adams LK, Lyon DY, McIntosh A, Alvarez PJJ. Comparative toxicity of nano-scale TiO_2, SiO_2 and ZnO water suspensions. Water Sci Technol 2006; 54: 327-334.

[13] Barnes RJ, Molina R, Xu J, Dobson PJ, Thompson IP. Comparison of TiO2 and ZnO nanoparticles for photocatalytic degradation of methylene blue and the correlated inactivation of gram-positive and gram-negative bacteria. J Nanoparticle Res 2013; 15: 1432-1439.

[14] Dindar B, Içli S. Unusual photoreactivity of zinc oxide irradiated by concentrated sunlight. J Photochem Photobiol A Chem 2001; 140: 263-268.

[15] Cells DS, Chandiran AK, Abdi-jalebi M, Nazeeruddin MK, Gra M. Analysis of electron transfer properties of ZnO and TiO_2 photoanodes for dye-sensitized solar cells. ACS Nano 2014; 8: 2261-2268.

[16] Sobus J, Burdzin G, Karolczak J, Anta JA, Zio M. Comparison of TiO_2 and ZnO solar cells sensitized with an indoline dye: time-resolved laser spectroscopy studies of partial charge separation processes. Langmuir 2014; 30: 2505-2512.

[17] Chieng BW, Loo YY. Synthesis of ZnO nanoparticles by modified polyol method. Mater Lett 2012; 73: 78-82.

[18] Memisoglu G, Varlikli C. Conventional and inverted hybrid UV-PDs based on solution processed PFE:ZnO active layer. IEEE Photonics Technol Lett 2015; 27: 537-540.

[19] Wang X, Huang J, Han S, Yu J. High photoresponse inverted ultraviolet photodectectors consisting of iridium phosphor doped into poly(N-vinylcarbazole) polymeric matrix. Appl Phys Lett 2014; 104: 173304-4.

[20] Chen KS, Zhang Y, Yip HL, Sun Y, Davies JA, Ting C, Chen CP, Jen AKY. Highly efficient indacenodithiophene-based polymeric solar cells in conventional and inverted device configurations. Org Electron 2011; 12: 794-801.

[21] Ali GM, Moore JC, Kadhim AK, Thompson C. Electrical and optical effects of Pd microplates embedded in ZnO thin film based MSM UV photodetectors: a comparative study. Sensors Actuators A Phys 2014; 209: 16-23.

[22] Bai Z, Yan X, Chen X, Zhao K, Lin P, Zhang Y. High sensitivity, fast speed and self-powered ultraviolet photodetectors based on ZnO micro/nanowire networks. Prog Nat Sci Mater Int 2014; 24: 1-5.

[23] Arredondo B, de Dios C, Vergaz R, Criado AR, Romero B, Zimmermann B, Würfel U. Performance of ITO-free inverted organic bulk heterojunction photodetectors: comparison with standard device architecture. Org Electron 2013; 14: 2484-2490.

[24] Al-Hardan NH, Abdullah MJ, Ahmad H, Aziz AA, Low LY. Investigation on UV photodetector behavior of RF-sputtered ZnO by impedance spectroscopy. Solid State Electron 2011; 55: 59-63.

[25] Martens H, Pasveer W, Brom H, Huiberts J, Blom P. Crossover from space-charge-limited to recombination-limited transport in polymer light-emitting diodes. Phys Rev B 2001; 63: 125328-7.

[26] Simon M. Sze KKN. Physics of Semiconductor Devices. 3rd Edition. New York, NY, USA: Wiley, 2006.

[27] Yang T, Cai W, Qin D, Wang E, Lan L, Gong X, Peng J, Cao Y. Solution-processed zinc oxide thin film as a buffer layer for polymer solar cells with an inverted device structure. J Phys Chem C 2010; 114: 6849-6853.

[28] Sung YM, Hsu FC, Chen YF. Improved charge transport in inverted polymer solar cells using surface engineered ZnO-nanorod array as an electron transport layer. Sol Energy Mater Sol Cells 2014; 125: 239-247.

[29] Sun Y, Seo JH, Takacs CJ, Seifter J, Heeger AJ. Inverted polymer solar cells integrated with a low-temperature-annealed sol-gel-derived ZnO film as an electron transport layer. Adv Mater 2011; 23: 1679-1683.